Utilization of Pathway Signatures to Reveal Distinct Types of B Lymphoma in the Eμ-*myc* Model and Human Diffuse Large B-Cell Lymphoma

Seiichi Mori,[1,2] Rachel E. Rempel,[1,2] Jeffrey T. Chang,[1,2] Guang Yao,[1,2] Anand S. Lagoo,[3] Anil Potti,[1,4] Andrea Bild,[1,2,5] and Joseph R. Nevins[1,2]

[1]Duke Institute for Genome Sciences and Policy; Departments of [2]Molecular Genetics and Microbiology, [3]Pathology, and [4]Medicine, Duke University Medical Center, Durham, North Carolina; and [5]Department of Pharmacology and Toxicology, University of Utah, Salt Lake City, Utah

Abstract

The Eμ-*myc* transgenic mouse has provided a valuable model for the study of B-cell lymphoma. Making use of gene expression analysis and, in particular, expression signatures of cell signaling pathway activation, we now show that several forms of B lymphoma can be identified in the Eμ-*myc* mice associated with time of tumor onset. Furthermore, one form of Eμ-*myc* tumor with pre-B character is shown to resemble human Burkitt lymphoma, whereas others exhibit more differentiated B-cell characteristics and show similarity with human diffuse large B-cell lymphoma in the pattern of gene expression, as well as oncogenic pathway activation. Importantly, we show that signatures of oncogenic pathway activity provide further dissection of the spectrum of diffuse large B-cell lymphoma, identifying a subset of patients who have very poor prognosis and could benefit from more aggressive or novel therapeutic strategies. Taken together, these studies provide insight into the complexity of the oncogenic process and a novel strategy for dissecting the heterogeneity of B lymphoma. [Cancer Res 2008;68(20):8525–34]

Introduction

Human cancer is characterized by substantial heterogeneity, resulting from the acquisition of multiple somatic genetic and epigenetic alterations. Numerous studies have focused on identifying the molecular and genetic distinctions associated with tumor aggressiveness, including cancers that exhibit early onset. One presumes that the heterogeneity of cancer phenotypes reflects and is ultimately derived from variation in the accumulation of oncogenic events. Genetically engineered mice have provided a useful model system to explore and dissect this complexity by providing one well-defined event that initiates the oncogenic process. Importantly, many studies show that the development of tumors in the genetically defined models nevertheless requires additional alterations for development of the full tumor phenotype.

MYC is deregulated in various human cancers, such as Burkitt lymphoma, breast cancer, and prostate cancer (1). In Burkitt lymphoma, virtually every case involves chromosomal translocation of the *myc* locus to the IgH-J segment (1), resulting in ectopic overexpression of the *MYC* transcript in B cells. In addition to rearrangement, nonrandom somatic mutations within the *myc* coding region, which include ones providing stabilization to the protein (2), have been observed. Burkitt-like (or atypical Burkitt) lymphoma and a fraction of diffuse large B-cell lymphoma (DLBCL) also feature *MYC* deregulation. Similar *Myc* translocations are frequently detected in murine plasmacytomas, as well (1). The diagnosis of Burkitt lymphoma relies on morphologic findings, including an extremely high mitotic rate and a starry sky appearance of reactive macrophages, immunophenotypes featuring germinal center B cells, and the cytogenetics described above (3).

The Eμ-*myc* transgenic mouse has provided a valuable model for the study of MYC-driven B-lymphoid tumors. Whereas Eμ-*myc* lymphomas are generally classified as lymphoblastic lymphomas, they do share histologic and cytologic features with Burkitt lymphoma (4–6). Nevertheless, it has been difficult to relate the Eμ-*myc* tumors to discrete MYC-driven human and murine lymphomas, because the lymphomas arising in this model exhibit pre-B, immature B, or mixed pre-B/immature B immunophenotypes (4) whereas human Burkitt lymphomas and murine plasmacytomas arise from more differentiated B cells, specifically germinal center B cells and plasma cells, respectively (1, 7, 8). More recently, an alternative mouse model to transgenic Eμ-*myc* was generated by the knock-in of a single *Myc* gene into the *Igh* locus. This model is similarly prone to a disease that resembles human Burkitt lymphoma in histology, although the tumor has naive B-cell character, suggesting that deregulated Myc can evoke phenotypes in a cell that diverge from its overt cell differentiation status (9).

Like most cancer models that are initiated by a defined genetic alteration, the development of lymphomas in the Eμ-*myc* mouse involves the acquisition of additional mutations, giving rise to heterogeneity of the resulting tumors that can serve as a model for the heterogeneity of human cancer. One reflection of this in the Eμ-*myc* model may be seen as a variable time of onset of tumor development. We have made use of expression profiling, together with previously developed expression signatures of oncogenic pathway deregulation, as an approach to characterize the heterogeneity associated with lymphoma development. The expression profile for tumors in this murine model reveals multiple types of lymphoma, including ones that have not been identified by conventional immunotyping methods, and coincides with time of disease onset. Moreover, the profile resembles that for subsets of human non–Hodgkin's B-cell lymphomas, although the specific B-cell stages from which the tumors arise vary. Furthermore,

Note: Supplementary data for this article are available at Cancer Research Online (http://cancerres.aacrjournals.org/).

Current address for S. Mori: Cancer Research Centre of Excellence, Genomic Oncology Programme, National University of Singapore, Centre for Life Sciences, Singapore.

Requests for reprints: Joseph R. Nevins, Duke University, 2121 CIEMAS Building, 101 Science Drive, Durham, NC 27708. Phone: 919-684-2746; Fax: 919-681-8973; E-mail: nevin001@mc.duke.edu.

doi:10.1158/0008-5472.CAN-08-1329

we find that the variable onset spectrum reflects tumor differentiation status and the activities of Myc, E2F, phosphatidylinositol 3′-kinase (PI3K), and nuclear factor-κB (NF-κB). These observations suggest that lymphomas developing in the Eμ-*myc* mouse model, whose phenotypes are linked with time of onset, can be useful as models for specific types of human lymphoma. Additionally, utilization of gene expression signatures reflecting various oncogenic pathway activities has provided an opportunity to further dissect the complexity of these lymphomas, revealing a subset of human DLBCLs with very poor prognosis.

Materials and Methods

Mouse strains and tumor monitoring. Mice were housed in a Duke University Medical Center Division of Laboratory Animal Resources facility, and experiments were approved by the Duke University Institutional Animal Care and Use Committee. The mice used for this study were Eμ-*myc* transgenic mice (4) of a mixed C57BL/6 × 129 background, which, based on breeding history, was predominantly C57BL/6.[6] The specific 129 substrain background was 129/OlaHsd for 30% of the tumors and 129/SvJae for 70% of the tumors. The Eμ-*myc* transgenics were monitored weekly to identify any mice with malignant disease. Mice were evaluated for any visible or palpable lumps, a hunched posture, tachypnea, a swollen belly, or ruffled fur and sacrificed promptly upon the appearance of any such symptoms. When tumor onsets are compared between the C57BL/6 × 129 mice and our stock Eμ-*myc* transgenic mice maintained exclusively in the C57BL/6 strain, there is a similar pattern with both early-onset and late-onset tumors evident (Supplementary Fig. S1). Lymphomas that emerged in lymph nodes were carefully dissected from sacrificed mice, washed in PBS, and frozen in liquid nitrogen or fixed in 10% formalin for histologic analysis. The frozen tissue provided material for microarray analysis.

Immunohistochemical and histologic analysis. We performed histologic and immunohistochemical analysis as described previously (10). Four-micron thick H&E-stained sections of formalin fixed tissue were examined by an experienced hematopathologist (A.S.L.). The diagnostic criteria were described previously (5). Antibodies used in this study were rat anti-mouse CD45R/B220 (a pan-B maker; SouthernBiotech), goat anti-mouse IgM (a pre-B/differentiated B marker; SouthernBiotech), rabbit anti-TdT (a pro-B marker; Supertechs), goat anti-mouse κ/λ (a differentiated B marker; SouthernBiotech), and rat anti-mouse CD138 (a plasma-cell marker; BD PharMingen).

Tissue culture and adenovirus procedures. The methods for culturing primary mouse embryonic fibroblasts (MEF) and adenoviral amplification, titration, and infection of cultured cells were as previously described (11, 12).

DNA microarray analysis. RNA was extracted from lymphoma samples or MEFs infected with adenoviruses using Qiagen RNeasy kits (Qiagen). RNA sample integrity was verified by agarose gel electrophoresis or by using an Agilent 2100 Bioanalyser. We prepared the targets for DNA microarray analysis and hybridized to Affymetrix Mouse 430 2.0 GeneChip arrays according to the manufacturer's instruction and as previously published. The method for cross-platform comparison across different versions of Affymetrix GeneChip arrays was described previously (12). Data has been deposited in GEO (GSE 7897).

Statistical analyses of microarray data. Analysis of expression data was described previously (12). In summary, we collected training sets consisting of gene expression values of samples where the phenotype of interest, either pathway activity or B-lymphocyte differentiation, was known. We created gene expression signatures by choosing the genes whose expression profiles across the training samples most highly correlated with the phenotype. Then, to predict the status of the phenotype on a tumor expression dataset, we fit a Bayesian probit regression model that assigned the probability that a tumor sample exhibited evidence of the phenotype, based on the concordance of its gene expression values with the signature. Hierarchical clustering and visualization were performed using Gene Cluster 3.0[7] and Java TreeView.[8] Genes and tumors were clustered by average linkage using uncentered correlation as the similarity metric. We evaluated the statistical relationship between sets of genes with significant Gene Ontology terms or transcription factor binding motifs using GATHER (13).[9] Standard Kaplan-Meier patient survival curves were generated using GraphPad's Prism software and compared using the log-rank test.

Signatures for tumor status. The expression signatures for the prediction of oncogene status have been generated in previous (11, 12) and present studies. To detect the E2F activity in mouse lymphocytes, we selected the E2F2 signature, which was generated by overexpression of E2F2 in mouse primary embryonic fibroblasts (11). We chose E2F2 over other members of the E2F family because it is expressed preferentially in murine lymphocytes.[10] For this study, we newly developed profiles for MYC expression using MEFs (data not shown). To generate profiles for pre-BI, large pre-BII, small pre-BII, immature B, and mature B cells, we used GEO dataset GSE272; for profiles of germinal center B and plasma cells from mouse lymphomas, we used GSE4142 (14, 15). The human germinal center B signature is derived from GSE2350 (16, 17).[11] To generate expression profiles of individual steps in B-cell differentiation, we included samples from the step of interest and compared against samples from nonadjoining steps. For instance, to obtain the profile that specifically distinguishes small pre-BII cells from cells at the other stages, we used the data of small pre-BII cells versus pre-BI and mature B cells, and for the plasma cell profile, we used the data of plasma cells versus naive and germinal center B cells. For human samples, we used MYC and E2F1 expression profiles (ref. 12; data not shown). The expression data for PI3K activation was described previously (18). To obtain the expression profile for tumor necrosis factor α (TNFα), we used already existing data (19).[12] To validate the TNFα signature, we used two more data sets downloaded from GEO.[13] Components positively regulated by TNFα were highly enriched for genes with NF-κB binding motifs (data not shown), and the activity of the TNFα pathway was suppressed by a dominant-negative form of I-κB kinase, an NF-κB pathway–specific suppressor in the dataset of GSE2624 (Supplementary Fig. S2). These results indicated that the gene expression profile elicited by TNFα treatment was likely to be mediated by cellular NF-κB activity (20, 21). For human B-cell malignancy data sets, we used GSE2350 (17) and GSE4475 (22), as they included expression data for Burkitt lymphoma and DLBCL. For further validation of oncogene pathway activity of DLBCL, we used a DLBCL data from Dana-Farber Cancer Center (23).[14] We confirmed that the profile for a particular oncogene was comparable across different species and cell types (12).

Western analysis. To assess alterations in c-Myc, p19ARF, Mdm2, and p53 protein expression, lymphoma samples were dissected from morbid mice and immediately frozen. Preparation of whole-cell extract and Western analysis were performed as previously described (24). One hundred micrograms of protein were used for the analyses. The antibody to detect c-Myc was N262 (Santa Cruz; 1:1,000); p19ARF was detected using the polyclonal antibody Ab-1 (Oncogene; 1:10,000), Mdm2 using the polyclonal antibody C-18 (Santa Cruz; 1:1,000), and p53 by the monoclonal antibody Ab-1 (Oncogene; 1:1,000). Equal protein loading was verified by staining blots with Ponceau Red.

Southern analysis. Genomic DNA was isolated from lymphomas and 10 μg digested with *Bam*H1, *Afl*II, or *Eco*RI. The probes used in this study were a p53 cDNA fragment, p19ARF exon 1B fragment (kindly provided by Dr. Charles Sherr), and a heavy chain J3-J4 joining region genomic fragment.

[6] R.E. Rempel, manuscript submitted.

[7] http://bonsai.ims.u-tokyo.ac.jp/~mdehoon/software/cluster

[8] http://jtreeview.sourceforge.net

[9] http://gather.genome.duke.edu/

[10] R.E. Rempel, unpublished data.

[11] http://www.ncbi.nlm.nih.gov/geo

[12] http://www.ncbi.nlm.nih.gov/geo; GSE2638 and 2639.

[13] http://www.ncbi.nlm.nih.gov/geo; GSE591 and 2624.

[14] http://www.broad.mit.edu/cgi-bin/cancer/publications/pub_paper.cgi?mode=view&paper_id=102

Results

Gene expression patterns reflecting time of tumor onset in Myc-induced lymphoma. Eμ-*myc* transgenic mice develop aggressive lymphomas with 100% penetrance (4). Whereas the expression of Myc is clearly critical for development of tumors in these mice, various observations point to the role of additional, somatically acquired mutations as necessary components of tumor development. Indeed, previous work has documented the occurrence of associated genetic and/or epigenetic alterations, particularly Ras and p53 mutations, which develop in multiple Myc-induced tumor models (25–29). In principle, variation in the nature of associated mutations could contribute to heterogeneity in the tumors that develop in the Eμ-*myc* mice. As one potential illustration of such variation, we have observed that the time of tumor onset can vary dramatically, ranging from as early as 32 days to over 600 days (Fig. 1*A*). Furthermore, an examination of time of tumor onset in a large cohort of animals (n = 265 with confirmed lymphoma) allowed us to observe a minor population of late-onset tumors that arose after 400 days (n = 27; 10.2%), not described in previous studies (30). We also noticed that the distribution of age of onset was broad (Fig. 1*A*), raising the possibility that there are several distinct tumor types that are linked with time of onset. Indeed, a combination of histologic and immunohistochemical analyses suggest distinct characteristics in the tumors arising early versus late. Histologically, most of the early-onset and several of the late-onset lymphomas exhibited a starry sky appearance due to tangible body macrophages engulfing apoptotic tumor cells, a characteristic feature of human Burkitt lymphoma. Immunohistochemically, these tumors had pre-B (B220 positive and κ/λ negative) or more differentiated B, including immature B (B220 positive and κ/λ positive), phenotypes (Supplementary Table S1). Among the tumors arising late, histologic analysis indicated a much higher proportion of differentiated B-cell lymphomas and several lymphomas derived from plasma cells or with plasma cell differentiation (Supplementary Table S1).

To provide a more global and unbiased examination of potential distinctions between tumors arising early and late, we performed genome-wide expression analyses of early-onset and late-onset lymphomas from Eμ-*myc* transgenic mice using expression microarrays. Total RNA was prepared from a collection of early-onset and late-onset tumors subjected to Affymetrix GeneChip assays (Supplementary Table S2) and then analyzed by unsupervised hierarchical clustering (Fig. 1*B*). This approach does not presume that there are differences in the biological samples but rather allows the gene expression data to reveal any distinctions. In fact, the clustering revealed four main tumor groups that largely coincided with the time of tumor onset. Cluster I contained 24 of 25 early-onset lymphomas and 11 late tumors, whereas the other late-onset lymphomas were classified into three small clusters (II, III, and IV). The genes in each tumor cluster essentially characterized the tumors according to B-cell differentiation status. For instance, cluster I tumors expressed pre-B markers, whereas genes commonly expressed across the late-onset clusters (II, III and IV) are preferentially expressed in differentiated B cells. Clusters II and IV expressed genes that are normally expressed in mature B cells. Cluster III tumors showed similarity in marker expression to the CD4-positive B-cell lymphomas that emerged in the Eμ-*bcl2* transgenic mice (31). Tumors belonging to the late tumor cluster IV overexpressed genes characteristic of terminally differentiated B cells (plasma cells) and tumors derived from plasma cells, termed plasmacytomas (Fig. 1*B*; Supplementary Table S3). Despite this diversity and consistent with original reports describing the model (4), 36 of 37 tumors assessed by Southern analysis of heavy chain immunoglobulin gene rearrangement were clonal. As well, the majority of tumors, either of early or late onset, had undergone the expected disruption of the ARF-Mdm2-p53 tumor suppressor pathway (data not shown; ref. 26).

Additional evidence suggesting differences in the early and late tumors with respect to lymphocyte differentiation was revealed through the use of gene expression signatures developed to be specific for B-lymphocyte developmental status (Supplementary Fig. S3*B*; Supplementary Tables S4 and S5). As anticipated from the gene expression data and immunohistochemical data, lymphomas exhibiting pre-B molecular signatures (pre-BI, large pre-BII, and small pre-BII) developed significantly earlier than tumors having more differentiated transcriptional phenotypes (immature B, mature B, and plasma cells; pre-B versus differentiated B; median, 69 days versus 403 days; $P < 0.0005$, Mann-Whitney U test). Whereas pre-B lymphomas usually predominate in the Eμ-myc transgenic mouse model, lymphomas with immature B and mixed pre-B/B phenotypes are also observed (4). In the C57BL/6 background, the percentage of lymphomas with pre-B versus immature B immunophenotype varies by original report (pre-B, 33–71%; immature B, 29–67%; refs. 30, 32–34). Both immunophenotypes have also been observed in the mixed C57BL/6 × 129 background (35, 36). Indeed, the gene expression analysis in this study revealed 30 (60%) and 8 (16%) of 50 lymphomas illustrate pre-B and immature B phenotypes, respectively (Supplementary Table S5). Our sampling for the microarray study made use of tumor samples from very early or late arising lymphomas so as to enhance the identification of distinct forms of disease. Whereas it is possible that there are additional subtypes within the intermediate time of onset group, other analyses suggest that there would be a mixture of the tumor types found in the early and late groups. Overall, our observations not only confirmed the reported heterogeneity seen in previous studies but also identified rare types, such as plasmacytomas, not previously seen (6).

Distinct patterns of cell signaling pathway activation characterize the two forms of Eμ-*myc* B lymphoma. We have recently described an approach to the analysis of tumor heterogeneity using gene expression signatures that reflect activation of various cell signaling pathways (11, 12). An expression signature is simply a representation of a biological state in the form of a pattern of gene expression unique to that circumstance. In this case, quiescent cells or cells expressing various oncogenic activities, such as Ras, Myc, E2F, and others, are used to develop signatures that predict activation of these pathways (12). Importantly, these signatures provide an opportunity to assess the state of these pathways in other samples, including tumor samples. Furthermore, one can look for structure in the dataset in the form of clusters exhibiting similar patterns of pathway activation, much the same as looking for patterns of gene expression. Indeed, our previous work has shown that patterns of pathway activation can identify subgroups of patients with distinct clinical outcomes.

As shown in Fig. 2, we made use of four pathway signatures relevant to the analysis of lymphoma based on previous work, as well as the gene expression data in Fig. 1*B*, Supplementary Fig. S4, and Supplementary Tables S6, S7, and S8 (35, 37, 38). Two major clusters were identified by this analysis, and once again, these reflected the time of onset of tumor formation. Cluster I, including

primarily the early-onset lymphomas, exhibited activation of the E2F, PI3K, and Myc pathways, which were reduced in the late-onset tumors. In contrast, the TNFα(NF-κB) signature was more prominent in cluster II, which included primarily the later onset tumors. Myc, E2F, and PI3K activities were negatively correlated with the date of onset in linear regression analysis, whereas the probability of TNFα was positively correlated with onset. Similarly, there were correlations for each oncogene activity (Supplementary Table S9).

Taken together, these results provide evidence for several forms of B lymphoma emerging from the Eμ-*myc* mouse model based on overall patterns of gene expression, as well as distinct patterns of pathway activity revealed by the pathway signatures.

Relationship of early-onset and late-onset Eμ-*myc* tumors to human lymphomas. The distinction seen in the early-onset versus late-onset Eμ-*myc* tumors is reminiscent of recent work that has described four gene expression signatures that distinguish human Burkitt lymphoma from DLBCL (39). These include signatures for MYC, germinal center B cells, MHC class I, and NF-κB. Given the apparent role of MYC in the early-onset tumors and the enrichment for NF-κB responsive genes in the late-onset tumors, we examined the extent to which the Eμ-*myc* lymphomas exhibited characteristics of human lymphomas. To do so, we developed expression signatures reflecting these four characteristic differences of Burkitt lymphoma versus DLBCL and directly characterized the Eμ-*myc* tumors. The development of signatures representative of germinal

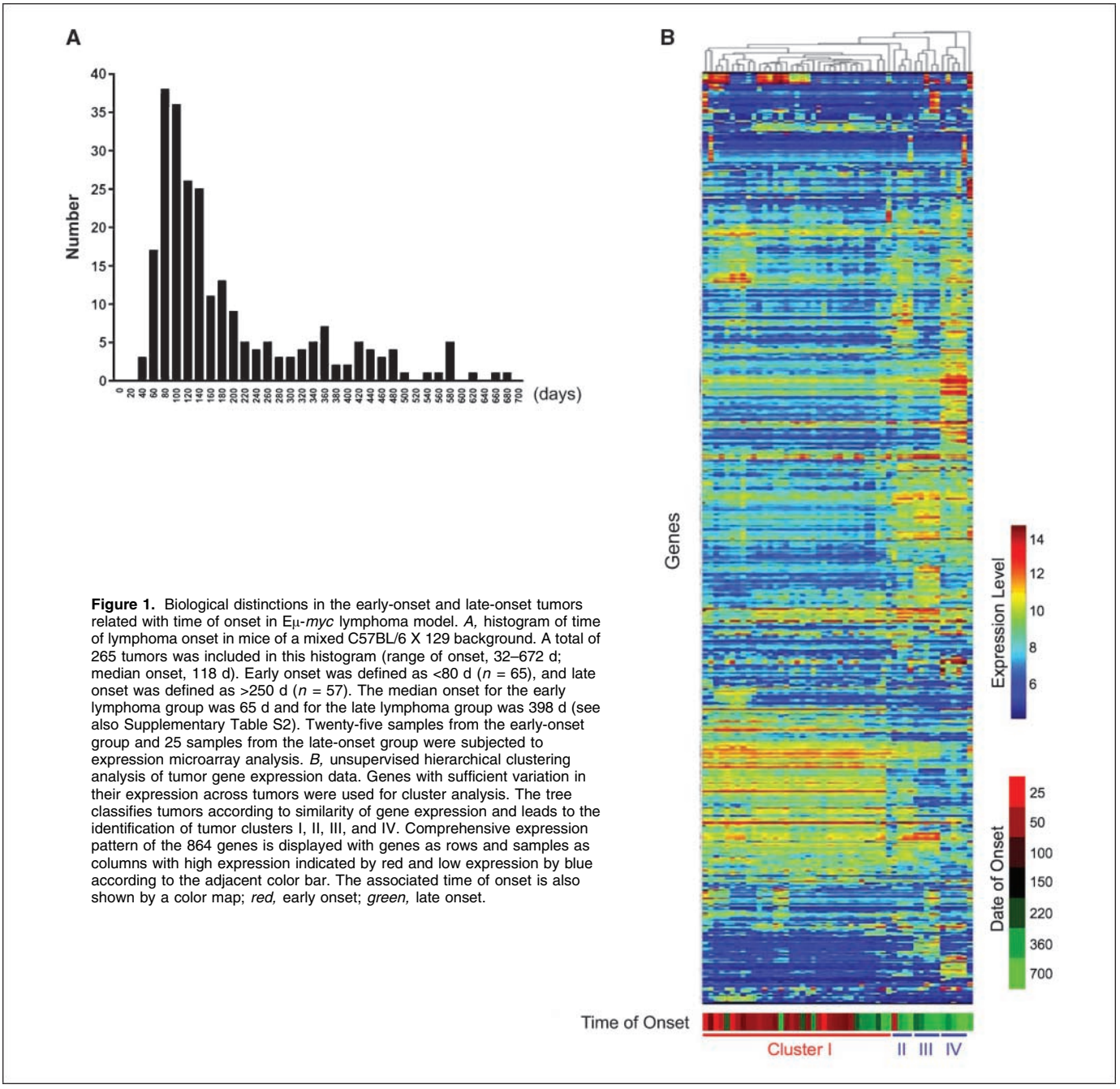

Figure 1. Biological distinctions in the early-onset and late-onset tumors related with time of onset in Eμ-*myc* lymphoma model. *A,* histogram of time of lymphoma onset in mice of a mixed C57BL/6 X 129 background. A total of 265 tumors was included in this histogram (range of onset, 32–672 d; median onset, 118 d). Early onset was defined as <80 d (n = 65), and late onset was defined as >250 d (n = 57). The median onset for the early lymphoma group was 65 d and for the late lymphoma group was 398 d (see also Supplementary Table S2). Twenty-five samples from the early-onset group and 25 samples from the late-onset group were subjected to expression microarray analysis. *B,* unsupervised hierarchical clustering analysis of tumor gene expression data. Genes with sufficient variation in their expression across tumors were used for cluster analysis. The tree classifies tumors according to similarity of gene expression and leads to the identification of tumor clusters I, II, III, and IV. Comprehensive expression pattern of the 864 genes is displayed with genes as rows and samples as columns with high expression indicated by red and low expression by blue according to the adjacent color bar. The associated time of onset is also shown by a color map; *red,* early onset; *green,* late onset.

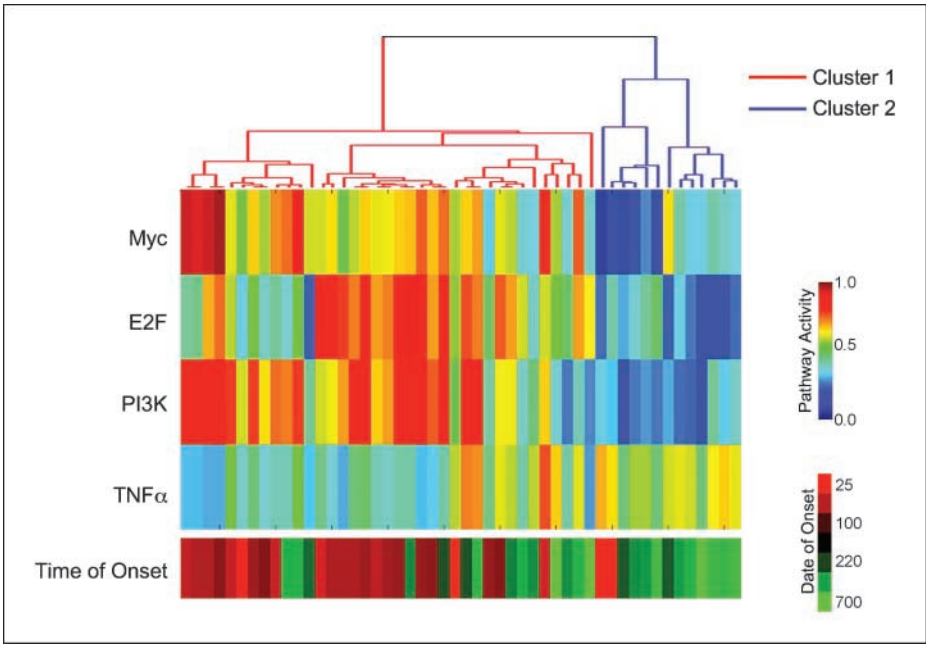

Figure 2. Patterns of pathway activation in Eμ-*myc* lymphomas. Signatures developed to predict the indicated pathways have been previously described. Additional signatures were developed as described in Materials and Methods. These were used to evaluate the status of the pathways in tumor samples as previously described. In each case, the probability of pathway activation was predicted from the signature and then displayed as a color map. Predicted probabilities were clustered by unsupervised hierarchical clustering. The color code indicates high (*red*) to low (*blue*) probability. Time of onset with associated sample IDs is shown by the adjacent color map; *red,* early onset; *green,* late onset.

center B cells, as well as the mean expression values of MHC class I genes, used available data as described in Materials and Methods. As shown by the analysis in Fig. 3*A*, these four gene expression signatures did indeed distinguish human Burkitt lymphoma from DLBCL. Consistent with previous reports, Burkitt lymphoma samples exhibited elevated MYC and germinal center B activities and DLBCL exhibited increased activities for MHC class I and TNFα (39).

We then applied these same four signatures to the samples of Eμ-*myc* tumors sorted on the basis of early or late onset. As shown in Fig. 3*B*, the Myc expression signature was elevated in the early-onset tumors, as well as the germinal center B-cell signature. Although most of early-onset lymphomas lacked germinal center B differentiation markers, such as CD10 and Bcl-6, and were characterized by pre-B marker expression (Supplementary Fig. S3*B* and Fig. 3; Supplementary Tables S3 and S5; data not shown), there was clearly an enrichment for the germinal center B-cell signature in these tumors. In contrast, the MHC class I and TNFα signatures were decreased in these early-onset tumors. The reverse pattern was seen for the late-onset tumors with elevated MHC class I and TNFα signatures and decreased Myc and germinal center B signatures. The expression signature of normal germinal center B cells can be dissected into multiple components reflecting B-cell differentiation status, as well as proliferative capacity (16, 40). As expected, human Burkitt lymphomas express higher levels of both of germinal center B-cell marker and proliferative genes than DLBCLs. Whereas the differentiation-specific genes are not evident in the murine early-onset tumors, the germinal center proliferative genes are clearly associated with these early-onset tumors (Fig. 3*C* and *D*). Taken together, this analysis provides evidence for distinct forms of B-cell lymphoma in the Eμ-*myc* model with characteristics of Burkitt lymphoma and DLBCL.

To further explore the relationship between Eμ-*myc* tumors and the Burkitt lymphoma versus DLBCL distinction, we reversed the analysis and made use of the gene expression data from the early-onset and late-onset Eμ-*myc* tumors to develop a specific signature reflecting the time of onset. We then used this signature to predict the status of the human B-cell lymphomas. To generate an early-versus-late signature, we used 30 samples that included the 15 earliest and 15 latest tumors (Fig. 4*A* and Supplementary Fig. 5). To validate the signature, we split the training samples into two subsets and found that both subsets have the capacity to predict time of onset accurately (Fig. 4*A*). Taken together, the gene expression analysis provides very clear evidence for at a minimum of two distinct types of tumors developing early and late in the Eμ-*myc* model, although late-onset lymphomas are further dissected into multiple subgroups (Fig. 1*B*). The more heterogeneity inside late-onset Eμ-*myc* lymphomas may be reminiscent to the disease complexity of human DLBCL that is further divided into multiple subgroups according to the morphologic or transcriptional characters (41).

We then used the early-versus-late signature developed from the Eμ-*myc* tumors to evaluate two separate collections of human lymphomas, making use of published datasets of microarray data for human Burkitt lymphomas and DLBCLs. As shown in Fig. 4*B*, this analysis revealed that human non–Hodgkin lymphomas with Burkitt or Burkitt-like morphology showed more similarity to mouse early-onset Myc-induced lymphoma, whereas lymphomas histologically diagnosed as DLBCL were similar to mouse late-onset lymphoma (Fig. 4*B*). Patient age at first diagnosis, which was available for GSE4475, was correlated by Spearman correlation with the molecular character for time-of-onset in mice, further validating murine early-versus-late signature and also supporting similar features of lymphoma in this mouse model and human disease (RS = -0.4209 and $P < 0.0001$).

Utilization of pathway signatures to further dissect lymphoma heterogeneity. The analyses shown in Figs. 2 and 3 highlight the capacity of pathway signatures to dissect tumor heterogeneity, revealing multiple classes of Eμ-*myc* lymphoma, as well as the distinctions between Burkitt lymphoma and DLBCL. In light of this, we have explored the potential of the pathway signatures to further dissect heterogeneity within populations of human lymphoma (GSE4475). As shown in Fig. 5*A*, this analysis revealed five distinct clusters of samples based on patterns of

pathway activity. Burkitt and Burkitt-like lymphomas had higher MYC, E2F, and PI3K probabilities and lower signals for the TNF signature, and conversely, TNF activity was higher in DLBCL samples. To further explore the biological significance of the pathway patterns in human lymphomas, we examined patient survival as a function of pathway cluster using Kaplan-Meier analysis. Whereas there was no significant difference in patient survival when comparing patient samples with high or low activity of a single-oncogene pathway predictor (data not shown), a subset of patients whose tumors exhibited intermediate activity for MYC, but low activity of the other pathways (Fig. 5*A*, cluster II), had a significantly worse prognosis than patients with other pathway patterns. We also compared the prognosis result based on pathway patterns to that achieved with conventional classification of DLBCL into ABC/GCB/Type 3 subclasses (7). This analysis shows that the subgroup identified based on a unique pathway pattern exhibits a prognosis as poor as the ABC subtype of DLBCL (GCB, hazard ratio = 0.609, $P = 0.055$; ABC, hazard ratio = 1.79, $P = 0.021$; Cluster II, hazard ratio = 3.05, $P = 0.00001$ by Cox regression model). Importantly, the samples in the poor prognosis group based on the pathway pattern include many from the GCB category, an otherwise good prognosis group. As such, this result suggests a capacity to further dissect DLBCL in a way not previously possible.

To evaluate the extent to which this pattern of pathway activity could reproducibly identify high-risk lymphoma patients, we carried out similar analyses using an independent set of DLBCL samples, which did not include Burkitt lymphoma samples (Dana-Farber DLBCL data; ref. 23). As shown in Fig. 5*B*, a similar pattern of pathway activity was seen in these samples, identifying a subgroup (cluster I in this case) with again the pattern of pathway activity that also coincides with poor prognosis. Once again, the survival of this group, which included patients categorized as GCB, was as poor as the clinically poor prognosis group of ABC patients (GCB, hazard ratio = 0.439, $P = 0.0023$; ABC, hazard ratio = 2.18, $P = 0.0076$; Cluster I, hazard ratio = 2.09, $P = 0.054$ by Cox regression model). Based on these analyses, we conclude that a unique pattern of pathway activation can identify a patient population with very poor prognosis as a subset of DLBCL not identified by other means, thus suggesting the potential to further dissect the heterogeneity of human B lymphomas using pathway status to reveal a clinically significant subset of patients.

Given the potential of the pathway patterns to identify an otherwise unrecognized high-risk population of DLBCL patients, we used this information to develop a predictor of poor prognosis that could be used in a clinical context. We used the pattern defined by the pathway signatures to serve as a training set to then use supervised methods of analysis to build a predictive model (Dana-Farber DLBCL data; Fig. 6*A*). This model was then applied to the data from the second dataset (GSE4475) as an independent validation opportunity. As shown in Fig. 6*B*, the model predicted the pathway pattern in the independent data with substantial accuracy and once again identified two distinct populations of patients with respect to overall survival.

Discussion

Whereas many studies point to the substantial complexity of human cancer and the capacity of genome-scale gene expression data to dissect this complexity, it has nevertheless often proved

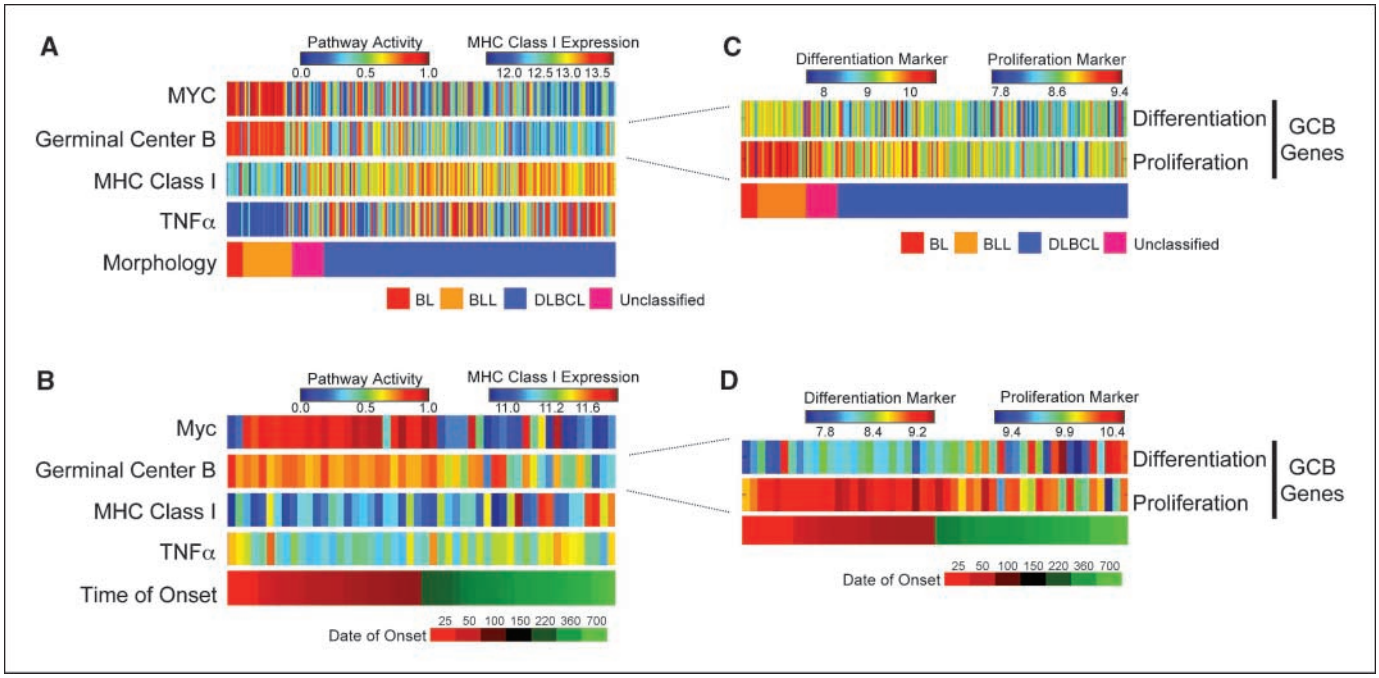

Figure 3. Pattern of four expression signatures that differentiate Burkitt lymphoma from DLBCL applied to Eμ-*myc* lymphoma samples. *A,* signatures representing MYC, germinal center B cells, and TNFα were used to predict the probability of activation of these pathways in human B lymphoma samples (GSE4475). In addition, mean expression values of MHC class I genes were measured. Each was illustrated by a heatmap. Color codes indicate high (*red*) or low (*blue*) probabilities or expression levels. *BL,* Burkitt lymphoma; *BLL,* Burkitt-like lymphoma. *B,* pattern of the four expression signatures in Eμ-*myc* lymphoma. Predicted probabilities (Myc, germinal center B, and TNFα) or mean expression values (MHC class I genes) are illustrated by a heatmap. Color codes indicate high (*red*) or low (*blue*) probabilities or expression levels. Time of onset is shown by the adjacent color map; *red,* early; *green,* late. *C* and *D,* dissection of the germinal center B signature. The mean expression levels for germinal center differentiation or proliferation maker genes are shown in the color map (*C,* GSE4475; *D,* Eμ-*myc* lymphoma). Gene lists for germinal center differentiation and proliferation were obtained from a previous expression microarray study (16). *BL,* Burkitt lymphoma; *BLL,* Burkitt-like lymphoma.

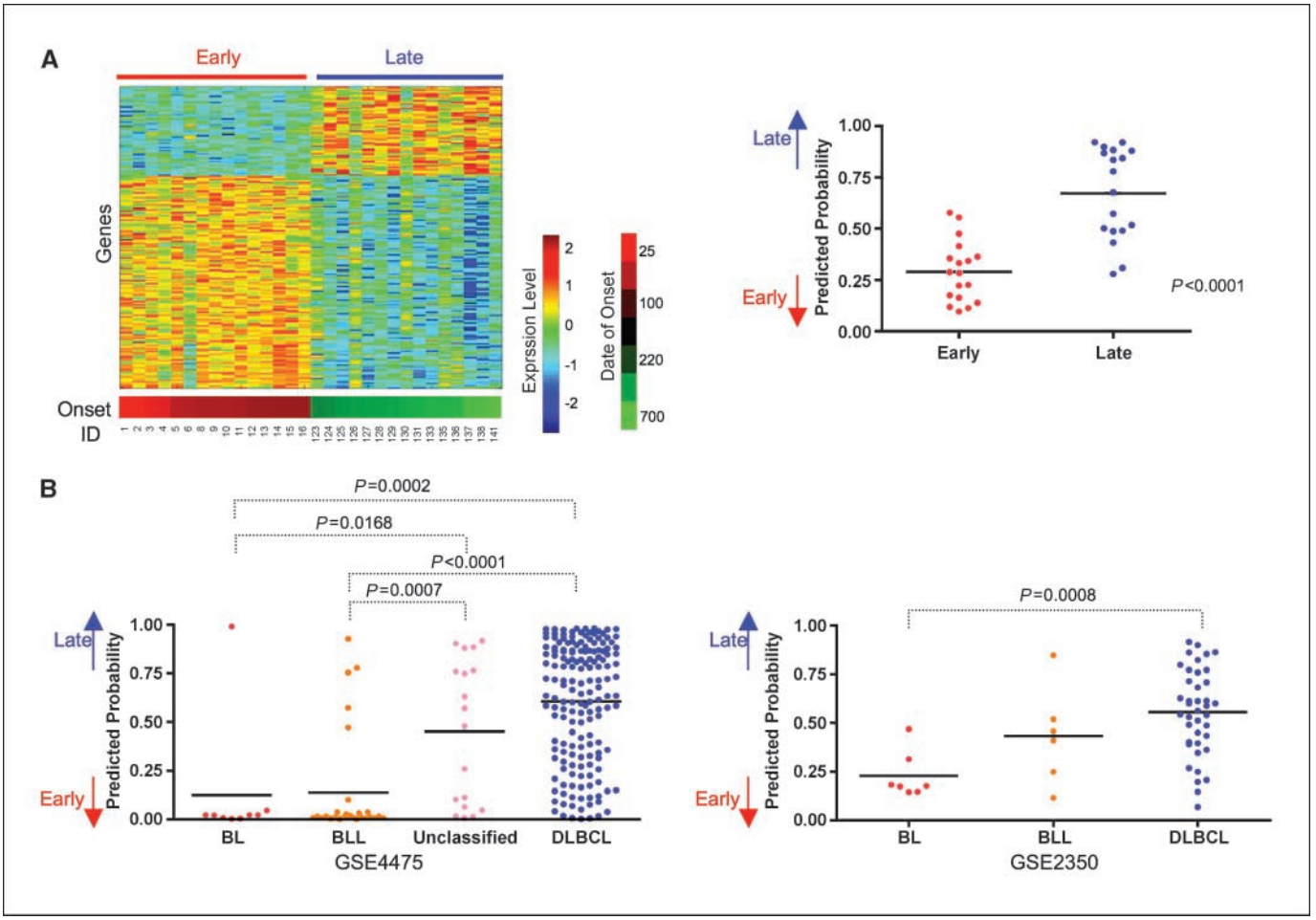

Figure 4. An expression signature that differentiates early-onset and late-onset Myc-induced lymphomas also distinguishes Burkitt lymphomas from DLBCLs. *A,* supervised analysis to generate a signature of early-versus-late lymphoma onset. *Left,* the expression pattern for the 200 selected genes that distinguish the earliest 15 versus the latest 15 mouse tumors. Expression levels are displayed with genes as rows and samples as columns and are illustrated by a heatmap. Time of onset is shown by the adjacent color map. Color codes indicate high (*red*) or low (*blue*) expression levels, or early (*red*) or late (*green*) lymphoma onset. Note that the earliest samples include 14 cluster I and 1 cluster II lymphomas, whereas the latest lymphomas were constituted by 3 cluster I, 3 cluster II, 3 cluster III, 4 cluster IV, and 2 unclassified tumors from Fig. 1*B*. *Right,* validation of the predictive capability of the early-versus-late signature. Using half the training samples, we predicted the status of the remaining 36 lymphomas. Predicted probabilities are then evaluated for the groups defined as early-onset and late-onset identified using Mann-Whitney *U* test. *Bar,* mean value for each group. The signature derived from the other half of the samples also provided statistically significant correlation for early-onset and late-onset tumors ($P = 0.0027$). *B,* predicted probabilities for early and late properties in human disease data sets that include Burkitt lymphomas and DLBCLs (*left,* GSE4475; *right,* GSE2350). Predicted probabilities are plotted for the groups with the defined morphology and statistically evaluated using Mann-Whitney *U* test. *Bar,* mean value for each group. *BL*, Burkitt lymphoma; *BLL,* Burkitt-like lymphoma.

difficult to interpret the underlying biology in these profiles. The approach we describe here takes an alternate strategy, one that makes use of expression signatures developed to reflect the activation or deregulation of various signaling pathways known to contribute to the oncogenic state to then characterize the heterogeneity seen in cancer. Using these signatures, we show that there are multiple distinct forms of B-cell lymphoma that in general coincide with time of onset that can be identified in the Eμ-*myc* mouse model. The pathway profiles revealed patterns distinct for the early-onset versus late-onset Myc-induced lymphomas, with characteristics reflecting the distinction between human Burkitt lymphoma and DLBCL.

Human non–Hodgkin's B-lineage lymphomas encompass numerous entities with variable clinical behavior and a range of distinctive molecular alterations that contribute to cellular phenotypes, such as growth potential and differentiation status. Recent studies using gene expression microarrays have revealed that Burkitt lymphoma, which belongs to the very aggressive lymphoma category, can be distinguished from DLBCL, which includes several entities with variable aggressiveness even in the cases that were difficult to diagnose by the conventional criteria (3, 39, 22). This distinction was based on the differential expression of four characteristic gene expression patterns reflecting MYC, germinal center B cells, MHC class I, and NF-κB. Our results suggest that the early-onset and late-onset mouse tumors have characteristics corresponding to human Burkitt lymphoma and DLBCL, respectively, with the early-onset tumors exhibiting elevation of signatures representing Myc and germinal center B cells, whereas the late-onset tumors reflect activation of NF-κB and MHC class I signatures. Given the fact that prognosis and chemotherapeutic strategies for the treatment of Burkitt lymphoma and DLBCL are significantly different and that there has not been an established mouse model that fully mimics either human Burkitt lymphoma or DLBCL, we suggest that the Eμ-*myc* mouse

could be exploited as a model system for the development of diagnostics and therapeutics for both diseases.

Although the expression signatures provide evidence for similarities between the early-onset Eμ-*myc* tumors and Burkitt lymphoma, one characteristic is inconsistent with this analogy. Various differentiation markers of germinal center B cells are not evident in many of the Eμ-*myc* tumors, including the early-onset tumors. Indeed, past work has generally concluded that the Eμ-*myc* mouse is not an appropriate model for human Burkitt lymphoma according to the discrepancy of their differentiation status (8). Nevertheless, the analysis of the four characteristic expression signatures, including that for germinal center B cells, was consistent with a pattern typical of human Burkitt lymphoma. Further dissection of the germinal center signature suggests a composite of genes reflecting differentiation status, as well as proliferative capacity. Whereas the differentiation-specific genes are not evident in the early-onset tumors, the germinal center proliferative genes are clearly associated with these early-onset tumors (Fig. 3). Interestingly, several cases of Burkitt lymphoma with pre-B immunophenotype have been reported in humans, implying that the status of germinal center B might not be a necessary condition for lymphomagenesis of human Burkitt lymphoma despite most of Burkitt lymphomas having germinal center B character (42–44). Considering the fact that pre-BCR signaling bears similarity with that of BCR (45), the pre-B state of Eμ-*myc* lymphoma undoubtedly shares some of the biological character of the BCR-activated germinal center B state of Burkitt lymphoma. We conclude that, whereas the human phenotypes are not perfectly reproduced in the differentiation status of several forms of the Eμ-*myc* tumors, a finding often seen with mouse models of human cancer, there are indeed clear characteristics of human Burkitt lymphoma and DLBCL evident in the early-onset and late-onset tumors.

Finally, the use of oncogenic pathway signatures has not only provided a characterization of the distinctions in the two forms of lymphomas emerging from the Eμ-*myc* mice but has also allowed a dissection of the complexity of the human B-cell lymphomas in a manner not previously possible. DLBCL is a heterogeneous disease with recognized variability in clinical outcome, genetic features, and cells of origin (23). Previous studies have focused on

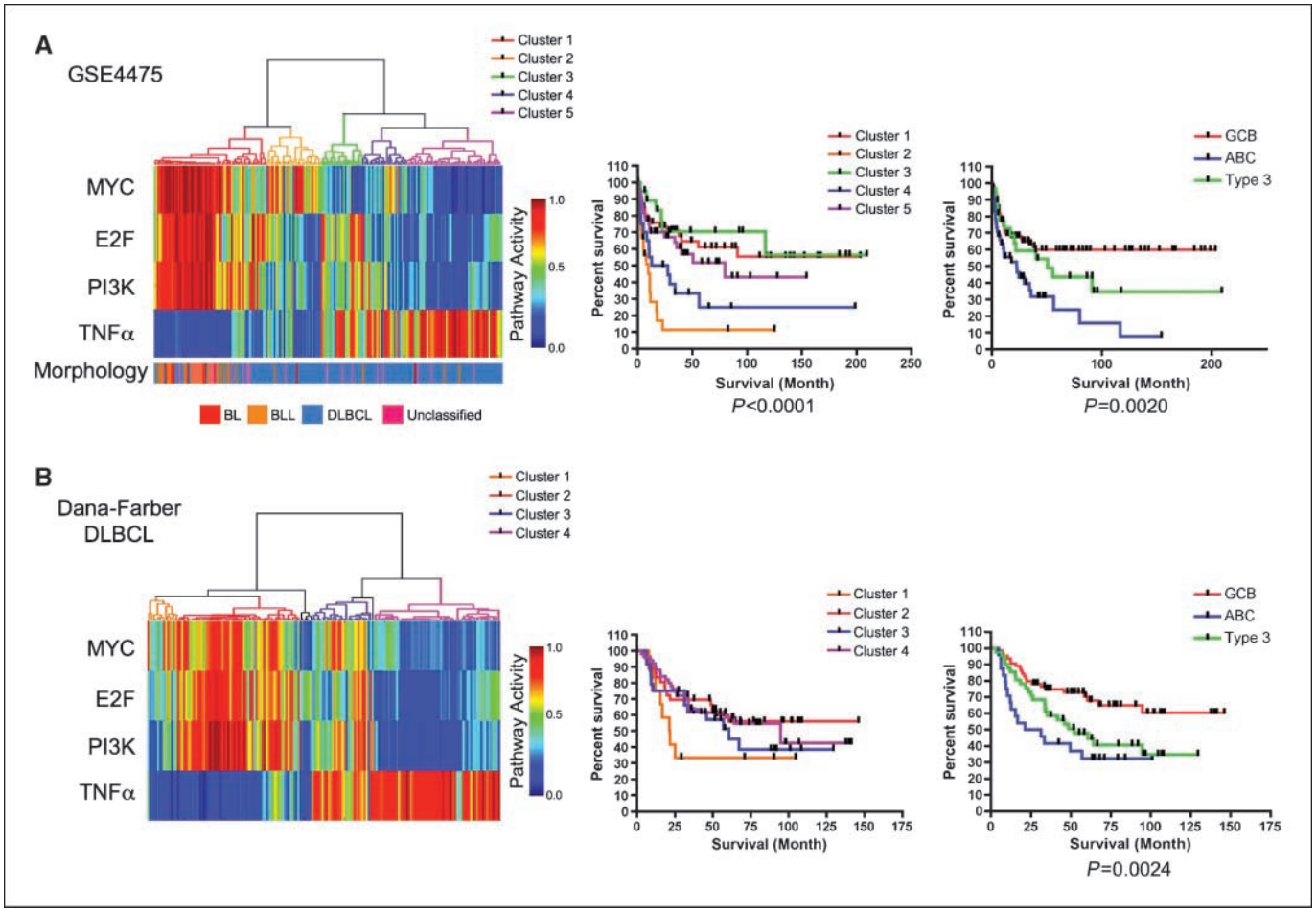

Figure 5. Utilization of oncogenic pathway signatures to identify subsets of human Burkitt lymphoma and DLBCL. *A* and *B, left,* cluster analysis for MYC, E2F, PI3K, and TNFα activities for human lymphomas. Predicted probabilities were clustered by unsupervised hierarchical clustering and are shown as a color map. The color maps indicate high (*red*) or low (*blue*) probabilities for the respective oncogenic pathways. Five (for GSE4475) or four (for Dana-Farber DLBCL data) tumor clusters, depicted as red, orange, green, blue, and purple, are identified. Associated morphologic information is color-coded below for GSE4475. Abbreviations for GSE4475 are the same as those in Fig. 3. *Middle,* Kaplan-Meier survival analysis based on pathway clusters (*A,* GSE4475; *B,* Dana-Farber DLBCL data). *Left and middle,* same color was used to depict a corresponding tumor subgroup in each dataset. *Right,* Kaplan-Meier survival analysis based on GCB-ABC classification (*A,* GSE4475; *B,* Dana-Farber DLBCL data). We used GCB-ABC labeling in the original articles (22, 23). In Kaplan-Meier analysis, tumor subgroups identified from clustering analysis were compared. The *P* value was calculated using the two-tailed log-rank test for all subgroups.

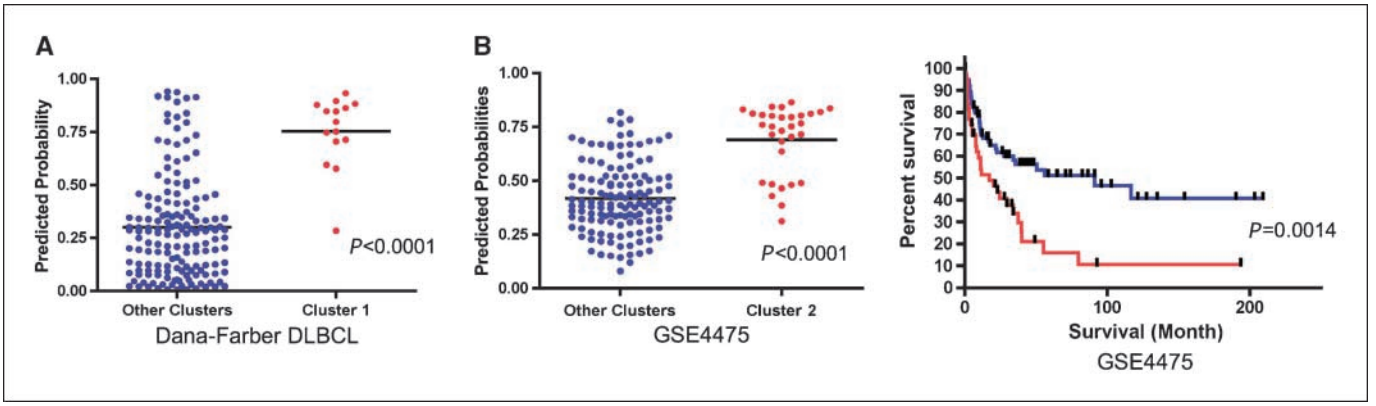

Figure 6. A pathway-specific predictor of poor prognosis in DLBCL patients. *A,* development of a pathway-specific predictor of poor prognosis. The pattern of MYC, E2F, PI3K, and TNFα identified as the poor prognosis group (cluster I in Fig. 5*B*) was used to fit a binary regression model as described in Materials and Methods. We then evaluated the predictive capacity using leave-one-out cross-validation. Mann-Whitney *U* test was used for statistical evaluation. *B,* validation of the poor prognosis predictor. The ability of the pathway-specific predictor to identify an independent group of patients as high risk, based on the pathway pattern, was evaluated in a second set of samples (GSE4475). *Left,* scatter plot for the predicted probabilities of the unique pathway pattern (cluster I of GSE4475). Mann-Whitney *U* test was used for statistical evaluation. *Right,* Kaplan-Meier analysis based on a single oncogene predictor activity. Samples with blue and red color are defined as being below and above 0.5 of predicted probabilities respectively.

an ability to dissect the subtypes of DLBCL, including ABC, GCB, and Type 3, in a more precise manner that provides a clear basis for prognosis. Our analysis using a collection of pathway signatures has identified a subset of DLBCL patients with poor prognosis based on a unique pathway pattern, not discernable based on other analyses, that emphasizes the power of this assay to further dissect cancer heterogeneity. Importantly, this subset of patients includes many that would be classified as GCB and thus conventionally with a relatively good prognosis. As such, the pathway-specific information provides an opportunity to refine current prognosis to select a group of patients who might be treated more aggressively based on the poor prognosis. Indeed, our ability to develop a pathway-specific signature that has the capacity to not only identify this subgroup but importantly to predict the subgroup provides a mechanism to use this information in clinical practice.

The information derived from these analyses goes further because, unlike overall gene expression data, the pathway analyses provide the opportunity to link patterns with potential therapeutic opportunities. Our previous work has shown the capacity of pathway signatures to predict sensitivity to drugs that target components of the relevant pathway (12, 18). Together with the known link between NF-κB activation and IκB-kinase inhibitors, and now a link between PI3K activation and PI3K inhibitors, in addition to the connection between E2F and cyclin-dependent kinase inhibitors, this information provides multiple opportunities to develop new therapeutic strategies across the spectrum of B lymphomas, guided by the prediction of pathway activation as described here.

Disclosure of Potential Conflicts of Interest

A. Bild: Speakers bureau/honoraria, Pfizer. The other authors disclosed no potential conflicts of interest.

Acknowledgments

Received 4/9/2008; revised 7/15/2008; accepted 7/29/2008.

Grant support: Award numbers R01CA106520 and U54CA112952 from the National Cancer Institute (J.R. Nevins). S. Mori was a research fellow of the Uehara Memorial Foundation.

The costs of publication of this article were defrayed in part by the payment of page charges. This article must therefore be hereby marked *advertisement* in accordance with 18 U.S.C. Section 1734 solely to indicate this fact.

We thank Drs. S. Dave, B. Weinberg, D. Rizzieri, H. Dressman, W. Quanli, E. Andrechek, D. Friedman, T. Fujimoto, M. Ogawa, N. Sakaguchi, Y. Yokota, S. Takao, S. Akiyama, T. Inoue, M. Oshimura, T. Baba, N. Matsumura, M. Araki, and H. Saya and members of Nevins laboratory for the critical reading of the manuscript and/or helpful discussions; S. Adler, K. Yu, D. Chasse, and L. Jakoi for help with experiments; and T. Henry and K. Culler for assistance with the preparation of the manuscript.

The content is solely the responsibility of the authors and does not necessarily represent the official views of the National Cancer Institute or the National Institutes of Health.

References

1. Nesbit CE, Tersak JM, Prochownik EV. MYC oncogenes and human neoplastic disease. Oncogene 1999;18:3004–16.
2. Sears R, Leone G, DeGregori J, Nevins JR. Ras enhances Myc protein stability. Mol Cell 1999;3:169–79.
3. Jaffe ES, Harris NL, Stein HJ, Vardiman JW. Tumours of haematopoietic and lymphoid tissues. Lyon (France): IARC Press; 2001.
4. Adams JM, Harris AW, Pinkert CA, et al. The c-myc oncogene driven by immunoglobulin enhancers induces lymphoid malignancy in transgenic mice. Nature 1985; 318:533–8.
5. Morse HC, Anver MR, Fredrickson TN, et al. Bethesda proposals for classification of lymphoid neoplasms in mice. Blood 2002;100:246–58.
6. Harris AW, Pinkert CA, Crawford M, Langdon WY, Brinster RL, Adams JM. The Eμ-myc transgenic mouse. A model for high incidence spontaneous lymphoma and leukemia of early B cells. J Exp Med 1988;167:353–71.
7. Shaffer AL, Rosenwald A, Staudt, LM. Lymphoid malignancies: the dark side of B-cell differentiation. Nature Rev 2002;2:920–32.
8. Kovalchuk AL, Qi CF, Torrey TA, et al. Burkitt lymphoma in the mouse. J Exp Med 2000;192:1183–90.
9. Zhu D, Qi CF, Morse HCI, Janz S, Stevenson FK. Deregulated expression of the Myc cellular oncogene drives development of mouse "Burkitt-like" lymphomas from naive B cells. Blood 2005;105:2135–7.
10. Mori S, Inoshima K, Shima Y, Schmidt EV, Yokota Y, Forced expression of cyclin D1 does not compensate for Id2 deficiency in the mammary gland. FEBS Lett 2003; 551:123–7.
11. Huang E, Ishida S, Pittman J, Dressman H, West M, Nevins JR. Gene expression phenotypic models that predict the activity of oncogenic pathways. Nat Genet 2003;34:226–30.
12. Bild A, Yao G, Chang JT, et al. Oncogenic pathway signatures in human cancers as a guide to targeted therapies. Nature 2006;439:353–7.
13. Chang JT, Nevins JR. GATHER: a systems approach to interpreting genomic signatures. Bioinformatics 2006;22: 2926–33.
14. Hoffmann R, Siedl T, Neeb M, Rolink A, Melchers F. Changes in gene expression profiles in developing B cells of murine bone marrow. Genome Res 2002;12: 98–111.

15. Luckey CJ, Bhattacharya D, Goldrath AW, Weissman IL, Benoist C, Mathis D. Memory T, memory B. cells share a transcriptional program of self-renewal with long-term hematopoietic stem cells. Proc Natl Acad Sci U S A 2006;103:3304–9.
16. Klein U, Tu Y, Stolovitzky GA, et al. Transcriptional analysis of the B cell germinal center reaction. Proc Natl Acad Sci U S A 2003;100:2639–44.
17. Basso K, Margolin AA, Stolovitzky G, Klein U, Dalla-Favera R, Califano A. Reverse engineering of regulatory networks in human B cells. Nat Genet 2005; 37:382–90.
18. Potti A, Lancaster JM, Dressman HK, et al. A genomic strategy to guide the use of chemotherapeutic drugs in solid tumors. Nat Med 2006;12:1294–300.
19. Viemann D, Goebeler M, Schmid S, et al. TNF induces distinct gene expression programs in microvascular and macrovascular human endothelial cells. J Leukoc Biol 2006;80:174–85.
20. Tian B, Nowak DE, Jamaluddin M, Wang S, Brasier AR. Identification of direct genomic targets downstream of the nuclear factor-κB transcription factor mediating tumor necrosis factor signaling. J Biol Chem 2005;280: 17435–48.
21. Tang Z, McGowan BS, Huber SA, et al. Gene expression profiling during the transition to failure in TNF-α over-expressing mice demonstrates the development of autoimmune myocarditis. J Mol Cell Cardiol 2004;36:515–30.
22. Hummel M, Bentink S, Berger H, et al. A biologic definition of Burkitt's lymphoma from transcriptional and genomic profiling. N Engl J Med 2006; 354:2419–30.
23. Monti S, Savage KJ, Kutok JL, et al. Molecular profiling of diffuse large B cell lymphoma identifies robust subtypes including one characterized by host inflammatory response. Blood 2005;105:1851–61.
24. Leone G, Sears R, Huang E, et al. Myc requires distinct E2F activities to induce S phase and apoptosis. Mol Cell 2001;8:105–13.
25. D'Cruz CM, Gunther EJ, Boxer RB, et al. c-MYC induces mammary tumorigenesis by means of a preferred pathway involving spontaneous Kras2 mutations. Nat Med 2001;7:235–9.
26. Eischen CM, Weber JD, Roussel MF, Sherr CJ, Cleveland JL. Disruption of the ARF-Mdm2–53 tumor suppressor pathway in Myc-induced lymphomagenesis. Genes Dev 1999;13:2658–69.
27. Schmitt CA, McCurrach ME, de Stanchina E, Wallace-Brodeur RR, Lowe SW. INK4a/ARF mutations accelerate lymphomagenesis and promoter chemoresistance by disabling p53. Genes Dev 1999;13:2670–7.
28. Alexander WS, Bernard O, Cory S, Adams JM. Lymphomagenesis in E mu-myc transgenic mice can involve ras mutations. Oncogene 1989;4:575–81.
29. He L, Thomson JM, Hemann MT, et al. A microRNA polycistron as a potential human oncogene. Nature 2005;435:828–33.
30. Egle A, Harris AW, Bouillet P, Cory S. Bim is a suppressor of Myc-induced mouse B cell leukemia. Proc Natl Acad Sci U S A 2004;101:6164–9.
31. Strasser A, Harris AW, Cory S. E mu-bcl-2 transgene facilities spontaneous transformation of early pre-B and immunoglobulin-secreting cells but not T cells. Oncogene 1993;8:1–9.
32. Scott CL, Schuler M, Marsden VS, et al. Apaf-1 and caspase-9 do not act as tumor suppressors in myc-induced lymphomagenesis or mouse embryo fibroblast transformation. J Cell Biol 2004;164:89–96.
33. Kelly PN, Puthalakath H, Adams JM, Strasser A. Endogenous bcl-2 is not required for the development of Emu-myc-induced B-cell lymphoma. Blood 2007;109: 4907–13.
34. Wen R, Chen Y, Bai L, et al. Essential role of phospholipase C γ 2 in early B-cell development and Myc-mediated lymphomagenesis. Mol Cell Biol 2006;26:9364–76.
35. Keller U, Nilsson JA, Maclean KH, Old JB, Cleveland JL. Nfkb 1 is dispensable for Myc-induced lymphomagenesis. Oncogene 2005;24:6231–40.
36. Alt JR, Greiner TC, Cleveland JL, Eischen CM. Mdm2 haplo-insufficiency profoundly inhibits Myc-induced lymphomagenesis. EMBO J 2003;22:1442–50.
37. Baudino TA, Maclean KH, Brennan J, et al. Myc-mediated proliferation and lymphomagenesis, but not apoptosis, are compromised by E2f1 loss. Mol Cell 2003; 11:905–14.
38. Schlee M, Holzel M, Bernard S, et al. C-myc activation impairs the NF-κB and the interferon response: implications for the pathogenesis of Burkitt's lymphoma. Int J Cancer 2007;120:1387–95.
39. Dave SS, Fu K, Wright GW, et al. Molecular diagnosis of Burkitt's lymphoma. N Engl J Med 2006;354:2431–42.
40. Ma C. Staudt LM. Molecular definition of the germinal centre stage of B-cell differentiation. Philos Trans R Soc Lond B Biol Sci 2001;356:83–9.
41. Shipp MA, Ross KN, Tamayo P, et al. Diffuse large B-cell lymphoma outcome prediction by gene-expression profiling and supervised machine learning. Nat Med 2002;8:68–74.
42. Ganick DJ. Finlay JL. Acute lymphoblastic leukemia with Burkitt cell morphology and cytoplasmic immunoglobulin. Blood 1980;56:311–4.
43. Mangan KF, Rauch AE, Bishop M, Spiers AS, Lorch C, Scharfman WB. Acute lymphoblastic leukemia of Burkitt's type (L-3 ALL) lacking surface immunoglobulin and the 8;14 translocation. Am J Clin Pathol 1985;83: 121–6.
44. Preud'homme JL, Dellagi K, Guglielmi P, et al. Immunologic markers of Burkitt's lymphoma cells. IARC Sci Publ 1985;60:47–64.
45. Melchers FB lymphocyte lineage cells from early precursors to Ig-secreting plasma cells: targets of regulation by the myc/mad/max families of genes? Curr Top Microbiol Immunol 1997;224:19–30.